

# Lattice dynamics of the heavy fermion compound URu<sub>2</sub>Si<sub>2</sub>

J. Buhot, M.A. Méasson,\* Y. Gallais, M. Cazayous, and A. Sacuto  
*Laboratoire Matériaux et Phénomènes Quantiques, UMR 7162 CNRS,  
 Université Paris Diderot, Bât. Condorcet 75205 Paris Cedex 13, France*

F. Bourdarot, S. Raymond, G. Lapertot, D. Aoki, and L.P. Regnault  
*SPSMS, UMR-E CEA / UJF-Grenoble 1, INAC, 38054 Grenoble, France*

A. Ivanov  
*Institut Laue Langevin, 38042 Grenoble, France*

P. Piekarczyk and K. Parlinski  
*Institute of Nuclear Physics, Polish Academy of Sciences, 31-342 Kraków, Poland*

D. Legut  
*Nanotechnology Centre, VSB-Technical University of Ostrava, Ostrava, Czech Republic*

C.C. Homes  
*Condensed Matter Physics and Materials Science Department,  
 Brookhaven National Laboratory, Upton, New York 11973, USA*

P. Lejay  
*Institut Néel, CNRS et Université Joseph Fourier, BP166, F-38042 Grenoble Cedex 9, France*

R.P.S.M. Lobo  
*LPEM, PSL Research University, ESPCI-ParisTech, 10 rue Vauquelin,  
 F-75231 Paris Cedex 5, France CNRS, UMR 8213, F-75005 Paris,  
 France Sorbonne Universités, UPMC Univ Paris 06, F-75005 Paris, France  
 (Dated: March 3, 2022)*

We report a comprehensive investigation of the lattice dynamics of URu<sub>2</sub>Si<sub>2</sub> as a function of temperature using Raman scattering, optical conductivity and inelastic neutron scattering measurements as well as theoretical *ab initio* calculations. The main effects on the optical phonon modes are related to Kondo physics. The B<sub>1g</sub> (Γ<sub>3</sub> symmetry) phonon mode slightly softens below ~100 K, in connection with the previously reported softening of the elastic constant, C<sub>11</sub> – C<sub>12</sub>, of the same symmetry, both observations suggesting a B<sub>1g</sub> symmetry-breaking instability in the Kondo regime. Through optical conductivity, we detect clear signatures of strong electron-phonon coupling, with temperature dependent spectral weight and Fano line shape of some phonon modes. Surprisingly, the line shapes of two phonon modes, E<sub>u</sub>(1) and A<sub>2u</sub>(2), show opposite temperature dependencies. The A<sub>2u</sub>(2) mode loses its Fano shape below 150 K, whereas the E<sub>u</sub>(1) mode acquires it below 100 K, in the Kondo cross-over regime. This may point out to momentum-dependent Kondo physics. By inelastic neutron scattering measurements, we have drawn the full dispersion of the phonon modes between 300 K and 2 K. No remarkable temperature dependence has been obtained including through the hidden order transition. *Ab initio* calculations with the spin-orbit coupling are in good agreement with the data except for a few low energy branches with propagation in the (a,b) plane.

## I. INTRODUCTION

After almost three decades<sup>1</sup> of intensive experimental and theoretical research, the nature of the ordered phase found in the Kondo system URu<sub>2</sub>Si<sub>2</sub> at temperature below T<sub>0</sub>=17.5 K remains to be unraveled<sup>2,3</sup>. Whereas appearing clearly in the thermodynamic and transport quantities<sup>1,4,5</sup>, the order parameter of this electronic hidden order (HO) state could not be determined by any usual or sophisticated experimental techniques<sup>6</sup>. Theoretical proposals are numerous, starting from itinerant or

localized picture for the 5f electrons<sup>7–16</sup>.

Particular features of the HO state have been determined. Inelastic neutron measurements<sup>6,17,18</sup> observe two magnetic excitations with a commensurate wave vector Q<sub>0</sub>=(1,0,0) and an incommensurate wave vector Q<sub>1</sub>=(1.4,0,0)≡(0.6,0,0), the first one being a fingerprint of the HO state<sup>19</sup>. A partial Fermi-surface gapping with a strong reduction of the carriers number occurs at T<sub>0</sub><sup>20,21</sup>. At higher temperature, a heavy-electron Kondo liquid regime emerges below ~100 K<sup>1,22,23</sup>. This cross-over temperature, observed in resistivity for instance, has been shown to be drastically reduced under high mag-

netic field<sup>24</sup> until the HO state vanishes at  $\sim 35$  T, suggesting that the Kondo liquid regime is a precursor of the HO state. It is well admitted that a Brillouin zone folding from a body center tetragonal (bct) to a simple tetragonal (st) phase occurs upon entering the HO state<sup>16,25,26</sup>. Recently, various experiments have identified a four-fold symmetry breaking upon entering the HO state<sup>27,28</sup> and orthorhombic static lattice distortion has been reported by Tonegawa et al.<sup>29</sup>.

The physics of URu<sub>2</sub>Si<sub>2</sub> being mainly electronic, the lattice properties have been hardly investigated. Raman scattering<sup>30</sup> mainly reported temperature dependence of the intensity of the fully-symmetric phonon mode and optical conductivity studies were mostly focused on the electronic properties. A more detailed study by ultrasonic measurements versus temperature and under high magnetic field<sup>31,32</sup> reported a softening of the elastic constant  $C_{11} - C_{12}$  below  $\sim 120$  K suggesting a  $B_{1g}$ -type (or  $\Gamma_3$ ) lattice instability in connection with the Kondo cross-over. Quite recently, an anomalous phonon softening below  $T_0$  in the  $[1,1,0]$  direction has been reported by inelastic neutron scattering<sup>33</sup>, calling on for further detailed studies.

We report here a comprehensive study of the lattice dynamics of URu<sub>2</sub>Si<sub>2</sub> from 300 K to 2 K; the optical phonon modes have been investigated by Raman scattering (section III) and infrared (IR) (section IV) spectroscopies, the dispersion of the phonon branches by inelastic neutron scattering (including polarization techniques) (section V), and *ab initio* calculations (section VI) were used for comparison with all measurements.

## II. PHONON MODES IN URu<sub>2</sub>Si<sub>2</sub> AND SELECTION RULES

The URu<sub>2</sub>Si<sub>2</sub> compound belongs to the tetragonal space group  $I4/mmm$  ( $D_{4h}$ ), with the U, Ru and Si atoms located at the 2a, 4d and 4e Wyckoff positions, respectively. From group symmetry analysis<sup>34</sup>, 8 zone center optical phonons are expected,  $A_{1g}$ ,  $B_{1g}$ ,  $2E_g$ ,  $2A_{2u}$  and  $2E_u$ . Table I reports all these phonon modes, their multiplicity and the motion of the atoms involved. Due to inversion center in URu<sub>2</sub>Si<sub>2</sub> elementary cell, the gerade (g) mode are Raman active and the ungerade (u) ones are IR actives. The corresponding atomic displacement patterns are sketched in Figure 1.  $A_{1g}$  and  $B_{1g}$  modes involve motions of the Si and Ru atoms, respectively, along the c-axis. The  $E_g$  modes correspond to the motions of Si and Ru atoms in the ab-plane. The IR active modes involve motions of all atoms along the c-axis for the  $A_{2u}$  modes and in the ab-plane for the  $E_u$  modes.

In optical measurements, all the symmetries have been probed by combining different orientations of the samples and/or different incident ( $\vec{e}_i$ ) and scattered ( $\vec{e}_s$ ) light polarizations. Both Raman and IR scattering probes excitation with a transferred wave vector  $\vec{Q}$  close to zero. To obtain the full dispersion of the optic and acoustic phonon

branches we have carried out inelastic neutron scattering (INS). Here the transverse or longitudinal character of the phonon modes has been obtained by using different configurations of scattering vector  $\vec{Q}$  as well as by comparison with the theoretical prediction for each branch.

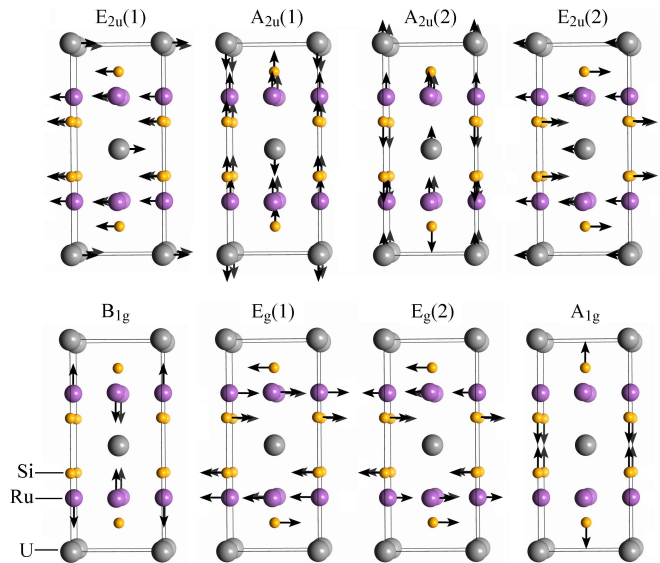


FIG. 1. (Color online) Atomic displacements sketches of the IR-active optical modes (up) and of the Raman-active optical modes (bottom) of URu<sub>2</sub>Si<sub>2</sub>. From the left to the right, the modes have increasing energy.

## III. RAMAN SPECTROSCOPY OF THE PHONONS

### A. Methods

Polarized Raman scattering has been performed in quasi-backscattering geometry with a incident laser line at 532 nm from a solid state laser. We have used a closed-cycle <sup>4</sup>He cryostat with sample in high vacuum ( $10^{-6}$  mbar) for the measurements from 8 K to 300 K and a <sup>4</sup>He pumped cryostat with the sample in exchange gas for measurements below 8 K or under magnetic field up to 10 T. By comparing Stokes and anti-Stokes Raman spectra and via the evolution of phonon frequencies with incident laser power, we have estimated the laser heating of the samples at +1.3 K/mW and +1 K/mW for the samples in high vacuum and in exchange gas, respectively. Typical laser power of 5 mW was used. The scattered light was analyzed by a Jobin Yvon T64000 triple subtractive grating spectrometer equipped with a cooled CCD detector. In the triple subtractive configuration we used, the resolution of the spectrometer is  $2.5 \text{ cm}^{-1}$ . For large energy scale measurements (up to  $3000 \text{ cm}^{-1}$ ), the spectrometer was used in the simple grating configuration, with a lower resolution. The contribution of the Bose factor has been removed for all spectra.

TABLE I. Raman and Infrared active modes for the Point Group  $D_{4h}$  ( $I4/mmm$ ) with corresponding irreducible representations, symmetry, atom displacements in  $URu_2Si_2$ .

Modes activity	Irreducible representation in Mulliken's notation	Corresponding symmetry in Bethe's notation (function)	Phonon Multiplicity	Atom displacements (direction)
Raman active	$A_{1g}$	$\Gamma_1^+ (x^2 + y^2, z^2)$	1	Si (c-axis)
	$A_{2g}$	$\Gamma_2^+ (J_z, ixy(x^2 + y^2))$	0	No active phonon
	$B_{1g}$	$\Gamma_3^+ (x^2 - y^2)$	1	Ru (c-axis)
	$B_{2g}$	$\Gamma_4^+ (xy)$	0	No active phonon
	$E_g$	$\Gamma_5^+ (xz, yz), (J_x, J_y)$	2	Si+Ru (ab-plane)
IR active	$A_{2u}$	$\Gamma_2^- (z)$	2	U+Ru+Si (c-axis)
	$E_u$	$\Gamma_5^- (x, y)$	2	U+Ru+Si (ab-plane)

### B. Sample preparation

The  $URu_2Si_2$  single crystals were grown by the Czochralski method using a tetra-arc furnace<sup>35</sup>. Two samples, from the same batch, were prepared. The initial residual resistivity ratio of the samples is about 50. Samples 1 and 2 were polished along the (a,c) and (a,a) planes, respectively. By cleaving, we obtained samples along the (a,a) plane. The  $E_g$  phonon modes can be probed only in (a,c) plane ( $\vec{E} // (a,c)$ ), so only on polished sample. Figure 2 shows the  $A_{1g}$  and  $B_{1g}$  phonon modes after polishing then after annealing, for sample 1 and for sample 2 (see inset). After polishing along the (a,c) plane (sample 1), both phonon modes are shifted by about 4% to higher energy and broadened. Most probably, the stress induced by polishing gives rise to such hardening and to the shortening of their lifetime. However, no such stress effect have been observed on the sample polishing along (a,a) plane (see inset of Figure 2). In order to release the stress induced by polishing, both samples have been annealed for two days at 950 ° under ultra high vacuum. This process has shifted down the phonon modes and it has clearly sharpened them. The final position and width are similar to what is measured on the cleaved sample of the same batch<sup>36</sup> (see inset of Fig.2) (Note that even sharper  $A_{1g}$  phonon mode with a full width at half maximum (FWHM) at 4 K of 4  $cm^{-1}$  have been measured on cleaved samples from another batch). The  $E_g$  modes measured on final sample 1 are very sharp, comparable to the resolution of the spectrometer at low temperature.

### C. Anharmonic model

The temperature dependence of the FWHM,  $\Gamma_{ph}$ , and energy,  $\omega_{ph}$ , of the phonon mode is usually described by a simple symmetric anharmonic decay model, i.e. decay of

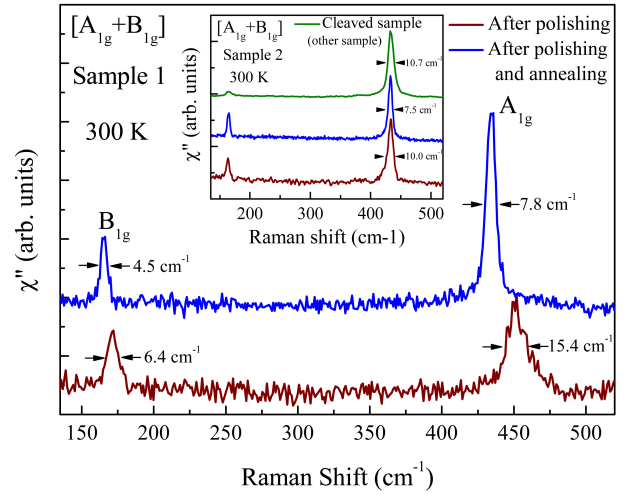


FIG. 2. (Color online) Raman spectra of  $URu_2Si_2$  for sample 1 after polishing along the (a,c) plane and annealing. Inset: Raman spectra for sample 2 after polishing along the (a,a) plane, annealing and for another sample cleaved along the (a,a) plane.

an optical phonon into two acoustic modes with identical frequencies and opposite momenta<sup>37,38</sup> :

$$\omega_{ph}(T) = \omega_0 - C \coth\left(\frac{\hbar\omega_0}{4k_B T}\right) \quad (1)$$

$$\Gamma_{ph}(T) = \Gamma_0 - \Gamma \coth\left(\frac{\hbar\omega_0}{4k_B T}\right) \quad (2)$$

where  $C$  and  $\Gamma$  are positive constants,  $\omega_0$  is the bare phonon frequency, and  $\Gamma_0$  a residual (temperature independent) linewidth originating from sample imperfections. With this purely phononic effect, upon cooling

down, the energy and the width of the phonon mode hardens and decreases, respectively, before saturating.

In addition, electron-phonon coupling can also induce renormalization of the frequency and width as well as a change of the shape of the phonon mode. In a simple model<sup>39,40</sup>, the width change is directly related to the electronic density at the energy of the phonon mode and the frequency relies on the full electronic spectrum. Generally, a loss of electronic density of states produces a narrowing of the phonon mode. Such coupling can also induce an asymmetric Fano shape of the phonon. If this last effect remains negligible, the line shape of the phonon can be described by a Lorentzian profile, i.e. :

$$\chi''(\omega) \propto \frac{\Gamma_{ph}/2}{(\omega - \omega_{ph})^2 + (\Gamma_{ph}/2)^2}$$

#### D. Results

Figure 3 shows typical Raman spectra obtained at 4 K on sample 1 after polishing and annealing.  $A_{1g}$  and  $B_{1g}$  phonon modes are visible in parallel polarization and  $E_g$  modes in cross-polarization. We observe a leakage of the  $A_{1g}$  mode in cross-polarization due to a weak crystal misalignment. At 300 K, the two  $E_g$  modes are seen at 213 and 391  $\text{cm}^{-1}$ , and  $A_{1g}$  and  $B_{1g}$  at respectively, 434 and 163  $\text{cm}^{-1}$ . The  $B_{1g}$  and both  $E_g$  phonon modes are sharper (with a FWHM of 3.2  $\text{cm}^{-1}$ , 2.8  $\text{cm}^{-1}$  and 1.8  $\text{cm}^{-1}$  at 4K, respectively) than the  $A_{1g}$  phonon mode (FWHM=6.6  $\text{cm}^{-1}$  at 4K). All phonons have a Lorentzian line shape.

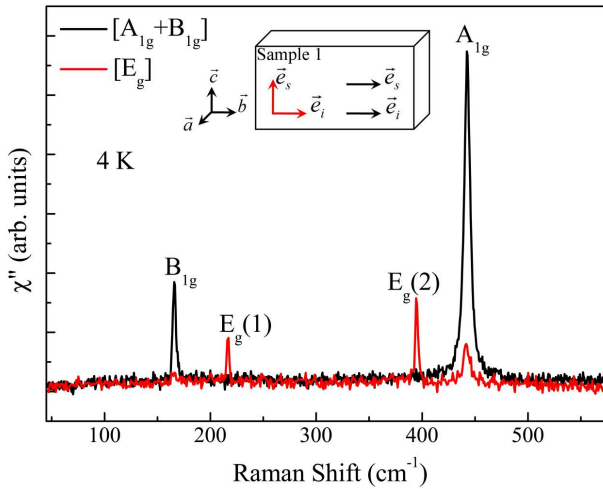


FIG. 3. (Color online) Typical Raman spectra measured at 4 K in cross and parallel polarization of the light and for sample 1. A scheme of sample 1 with the orientation of the polarizations of the incident  $\vec{e}_i$  and scattering  $\vec{e}_s$  light is shown.

Figure 4 and 5 present the temperature dependence of the energies and FWHM of the Raman-active phonon

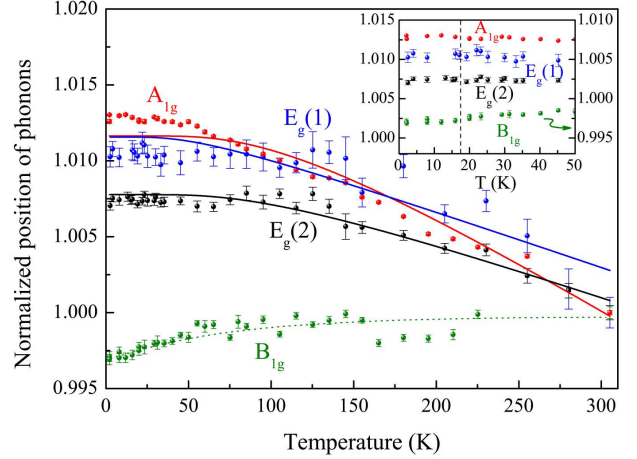


FIG. 4. (Color online) Temperature dependence of the position of the  $A_{1g}$ ,  $E_g(1)$ ,  $E_g(2)$  and  $B_{1g}$  phonon modes normalized to their value at 300 K.  $A_{1g}$  and  $E_g$  phonon modes have a typical temperature dependence whereas the  $B_{1g}$  phonon exhibits an unusual softening when cooling down below 100 K. Error bars have been extracted from the Lorentzian fits. Lines are fits with a single anharmonic model (see section III C). The green dot line is a guide to the eyes. Inset : zoom below 50 K across the hidden order transition marked by the vertical black dashed line. No particular anomaly is measured at  $T_0$ .

modes. The energies are normalized to their value at 300 K. We have investigated precisely the energy of the phonons through the hidden order transition but no particular effect has been observed within our accuracy (see inset of Figure 4). The energy of the  $A_{1g}$  mode increases with decreasing temperature before saturating at 1.25% higher energy than at 300 K. It narrows upon cooling before saturating. The general temperature dependence of this mode is naturally explained by anharmonic effects (full line are fits with the anharmonic model described in section III C). Other ingredients, like anharmonic effect of higher rank (four-phonon process), would be necessary to accurately fit the data.

The temperature dependence of the  $A_{1g}$  mode energy is consistent with previous Raman experiments<sup>41</sup>. No particular change of the integrated intensity of the  $A_{1g}$  phonon mode has been detected contrary to what Cooper et al. have reported<sup>41</sup>. Nor do we see any abrupt increase of the linewidth of  $A_{1g}$  below 20 K contrary to what is reported by Lampakis et al.<sup>42</sup>.

Whereas both  $E_g$  modes exhibit usual increasing energy when cooling down, their FWHM are almost constant in all the temperature range with a slight sharpening below  $\sim 20 - 30$  K. Within our accuracy, the increase of the lifetime of these phonons might be concomitant with the electronic gap opening at  $T_0$  observed by optical conductivity<sup>20,43-45</sup> and Raman scattering<sup>26</sup>. If so, a simple electron-phonon coupling model<sup>39,40</sup> would qualitatively explain such behavior.

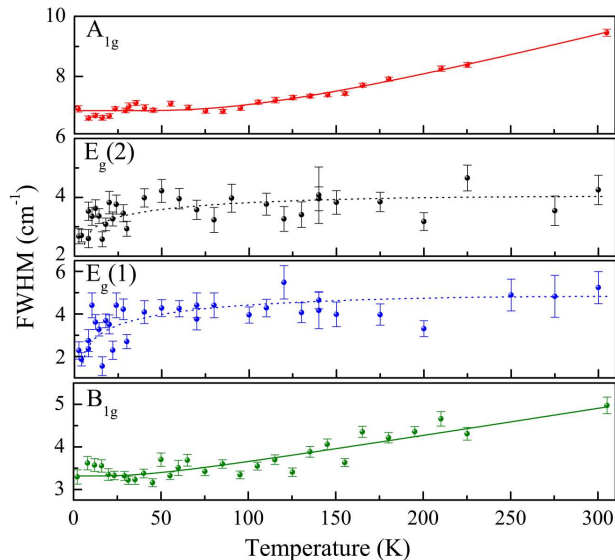


FIG. 5. (Color online) Temperature dependence of the FWHM of  $A_{1g}$ ,  $E_g(1)$ ,  $E_g(2)$  and  $B_{1g}$  phonon modes. Lines are fits with a single anharmonic model (see section III C). Dot lines are guides to the eyes.

Intriguingly, whereas the FWHM of the  $B_{1g}$  phonon shows the usual temperature evolution with narrowing when temperature decreases, its energy remains constant down to about 100 K before softening by about 0.5% below. This softening occurs in the temperature range of the Kondo cross-over and upon entering the Kondo liquid regime below the Kondo temperature reported between 70 K<sup>1,22</sup> and 120 K<sup>23</sup>. Clearly, the temperature dependence of the energy of the  $B_{1g}$  phonon cannot be reproduced by the simple anharmonic model. Moreover, contrary to what we observe, a simple electron-phonon coupling model generally predicts a change of the width as an initial effect on top of which the energy of phonon can be modified. We will further discuss this  $B_{1g}$ -symmetry softening in section III E.

A large energy scale investigation in all symmetries reveals three new peaks in  $A_{1g}$  symmetry, as shown Figure 6. In  $A_{1g} + B_{2g}$  symmetry three broad peaks appear at 350, 760 and 832  $\text{cm}^{-1}$  with a linewidth of 21, 37 and 37  $\text{cm}^{-1}$ , respectively. A slight hardening is observed with decreasing temperature. These new excitations are of pure  $A_{1g}$  symmetry as they are not observed in the  $B_{1g} + B_{2g}$  symmetry (not shown). These broad features could be due to crystal electric field excitations or double phonon processes. Because of a good agreement with theoretical calculation (see section VI), we attributed them to this last process. Indeed as shown in Figure 6 and 14, the energy ranges of the peaks (grey areas) are consistent with double excitations, either pure or mixed, of the  $B_{1g}$ ,  $E_g$  or  $A_{1g}$  branches.

Finally, we have probed all phononic excitations under high magnetic field up to 10 T (not shown). No effect has been observed.

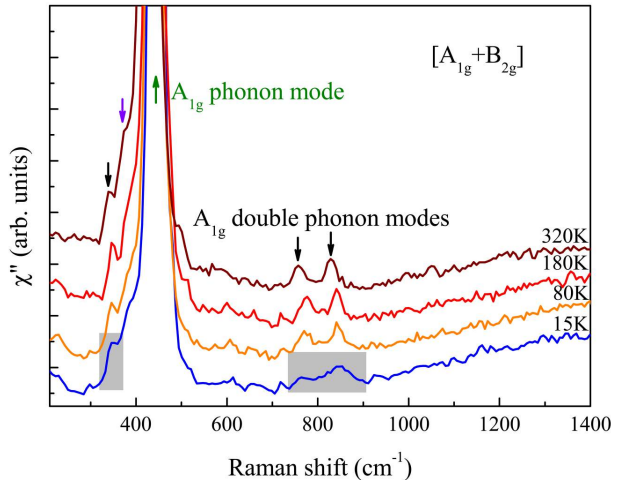


FIG. 6. (Color online) Large energy scale Raman spectra in  $A_{1g} + B_{2g}$  symmetry at various temperatures. Spectra have been shifted for clarity. Green arrow points to the center of the  $A_{1g}$  phonon mode. A leakage of the  $E_g(2)$  phonon mode is measured at about 394  $\text{cm}^{-1}$  (purple arrow). Three new broad peaks at about 350  $\text{cm}^{-1}$  and 800  $\text{cm}^{-1}$  are indicated by black arrows. Grey areas indicate the energy range for double phonon processes scattering according to theoretical calculations (see section VI and Fig.14). The three double phonon peaks are of pure  $A_{1g}$  symmetry.

## E. Discussion

Our most noticeable result of the Raman scattering investigation is the unusual temperature dependence of the energy of the  $B_{1g}$  phonon mode with softening below the Kondo temperature. The  $B_{1g}$  mode breaks the four-fold rotational symmetry. So the behavior of this  $B_{1g}$  phonon suggests a tendency toward lattice instability with orthorhombic distortion. Four-fold symmetry breaking and even orthorhombic distortion upon entering the HO state have been reported by various experiments<sup>27–29</sup>. However, the symmetry broken here is  $B_{2g}$ , i.e.  $45^\circ$  from the  $B_{1g}$  symmetry, both being in the (a,b) plane. Moreover, the temperature ranges are claimed to be different. Clearly, there is no direct relationship between these measurements and our Raman scattering result. The tendency toward lattice instability with  $B_{1g}$  symmetry is most probably related with the Kondo physics. Interestingly, similar softening effect (of 0.7%) of the elastic constant  $(C_{11} - C_{12})/2$  in the same symmetry ( $B_{1g} \equiv \Gamma_3$ ) has been reported below 120 K by ultrasound velocity measurements<sup>31</sup>. In addition, they show that this effect disappears when high magnetic field of 35 T is applied along the c axis. At this magnetic field, the coherence temperatures are strongly reduced concomitantly with the vanishing of the hidden order phase<sup>24</sup>. The softening of the elastic constant  $(C_{11} - C_{12})/2$  has been related to the emergence of the hybridized electronic state between the 5f electron and the conduction electrons (s or d)



and associated to a symmetry-breaking band instability. Both results, on acoustic (ultrasound experiment) and optical phonon (Raman experiment) modes, are nicely consistent and point to a  $B_{1g}$  symmetry-breaking instability upon entering into the Kondo regime of  $URu_2Si_2$ . While the acoustic phonon modes involve the motion of all atoms, the  $B_{1g}$  mode involves only the Ru atoms. This may suggest that the electronic environment of the Ru atoms are particularly affected by the Kondo physics.

On the basis of our inelastic neutron scattering study and theoretical calculations, we conclude that two origins for this small  $B_{1g}$  lattice instability are unlikely. First, our theoretical calculations including global anharmonic effects from purely phononic origin (See Section VI and Figure 15) indicates that none of the phonon branches, except the  $A_{2u}$  one, are strongly affected by these anharmonic effects. Secondly, by following the full dispersion of the " $B_{1g}$ " branch as well as magnetic excitations by inelastic neutron scattering (See V) we show that the  $k$ -dependence of the phonon is smooth going through the minima in the magnetic dispersion ( $\vec{Q}_0$  and  $\vec{Q}_1$ ). This does not give any indication of magneto-elastic coupling. Finally, as the  $B_{1g}$  mode is not affected by the large loss of carriers upon entering the HO state, as the phenomenon which induces the unusual  $B_{1g}$  energy behavior does not involve any noticeable change of its FWHM, a complex electron-phonon coupling related to the Kondo physics is certainly in play for this  $B_{1g}$  mode.

## IV. OPTICAL CONDUCTIVITY OF PHONONS

### A. Methods

Unpolarized optical reflectivity was measured on a cleaved  $2 \times 3 \text{ mm}^2$  ( $a, a$ ) plane. The  $c$ -axis reflectivity was taken with appropriate polarizers on sample 1 (see section III), an optically polished  $1 \times 1.5 \text{ mm}^2$  ( $a, c$ ) surface. We checked that the data along the  $a$  direction at 5 K was identical for unpolarized measurements on the ( $a, a$ ) plane and  $a$ -polarized measurements on the ( $a, c$ ) surface. Spectra were recorded at several temperatures from 5 K to 300 K, between  $20 \text{ cm}^{-1}$  (2.5 meV) and  $12\,000 \text{ cm}^{-1}$  (1.5 eV). This data was extended to  $40\,000 \text{ cm}^{-1}$  (5 eV) at room temperature. To obtain the absolute reflectivity we utilized an *in-situ* overfilling (gold or aluminum) evaporation technique.<sup>46</sup> In order to obtain the optical conductivity from Kramers-Kronig, we took a Hagen-Rubens extrapolation below our lowest measured frequency. Above  $40\,000 \text{ cm}^{-1}$ , we utilized the data by Degiorgi *et al.*<sup>47</sup> up to  $100\,000 \text{ cm}^{-1}$  (12 eV), followed by a  $\omega^{-4}$  free electron termination.

### B. Data modeling

In this paper, we are interested in the real part of the optical conductivity ( $\sigma_1$ ), which is built upon the sum of

the contributions from individual excitations:

$$\sigma_1 = \sigma_1^c + \sum_b \sigma_1^b + \sum_p \sigma_1^p, \quad (3)$$

where the superscripts  $c$ ,  $b$  and  $p$  stand for contributions from coherent mobile charge carriers, interband transitions, and phonons, respectively.

We describe the coherent part by a Drude conductivity in the form

$$\sigma_1^c(\omega) = \frac{2\pi}{Z_0} \frac{\Omega_p^2}{\omega^2 \tau + \frac{1}{\tau}}, \quad (4)$$

where  $\Omega_p$  is a plasma frequency,  $\tau^{-1}$  the scattering rate, and  $Z_0$  the vacuum impedance. Both, interband and phonon contributions can be modeled by Lorentz oscillators

$$\sigma_1^{b,p}(\omega) = \frac{2\pi}{Z_0} \frac{\gamma \omega^2 \Delta \epsilon \Omega^2}{(\Omega^2 - \omega^2)^2 + \gamma^2 \omega^2}, \quad (5)$$

where each contribution has a resonance frequency  $\Omega$ , a linewidth  $\gamma$ , and a dielectric oscillator strength  $\Delta \epsilon$ .

The Lorentz model does not take into account coupling between localized (*e.g.* phonon) states and the continuum. Fano<sup>39</sup> described phonon lineshapes in a conducting medium, when an electron-phonon coupling exists. Here we adopt the formalism proposed by Davis and Feldkamp<sup>48</sup>, who generalized Fano's approach to multiple discrete states:

$$\sigma_1^F = \frac{2\pi}{Z_0} R \omega \left\{ \frac{[q\gamma + (\omega - \Omega)]^2}{\gamma^2 + (\omega - \Omega)^2} - 1 \right\}, \quad (6)$$

where two new quantities are introduced.  $R$  is a renormalization parameter that takes into account the transition rate between continuum and localized states. But more interesting is the Fano-Breit-Wigner  $q^{-2}$ , which vanishes when the electron-phonon interaction disappears. It probes the continuum density of states at the phonon frequency.

### C. Results & Discussion

Figure 7 shows the optical conductivity around each phonon for both polarizations. We do observe all predicted modes by group theory: 2  $E_u$  phonons in the ( $a, a$ ) plane [panels (a) and (b)] and 2  $A_{2u}$  modes along the  $c$ -direction [panels (c) and (d)]. This is the first observation of the very weak  $A_{2u}$  phonon at  $115 \text{ cm}^{-1}$ , which we could only detect at low temperatures. Above  $\sim 30 \text{ K}$ , this phonon becomes too broad to be resolved in the spectra.

In panels (a) through (d) the symbols are the data and the solid lines are fits utilizing a Drude-Lorentz approach (Eqs. 4 and 5). To describe the continuum, we fitted the data to one Drude peak and two broad Lorentz

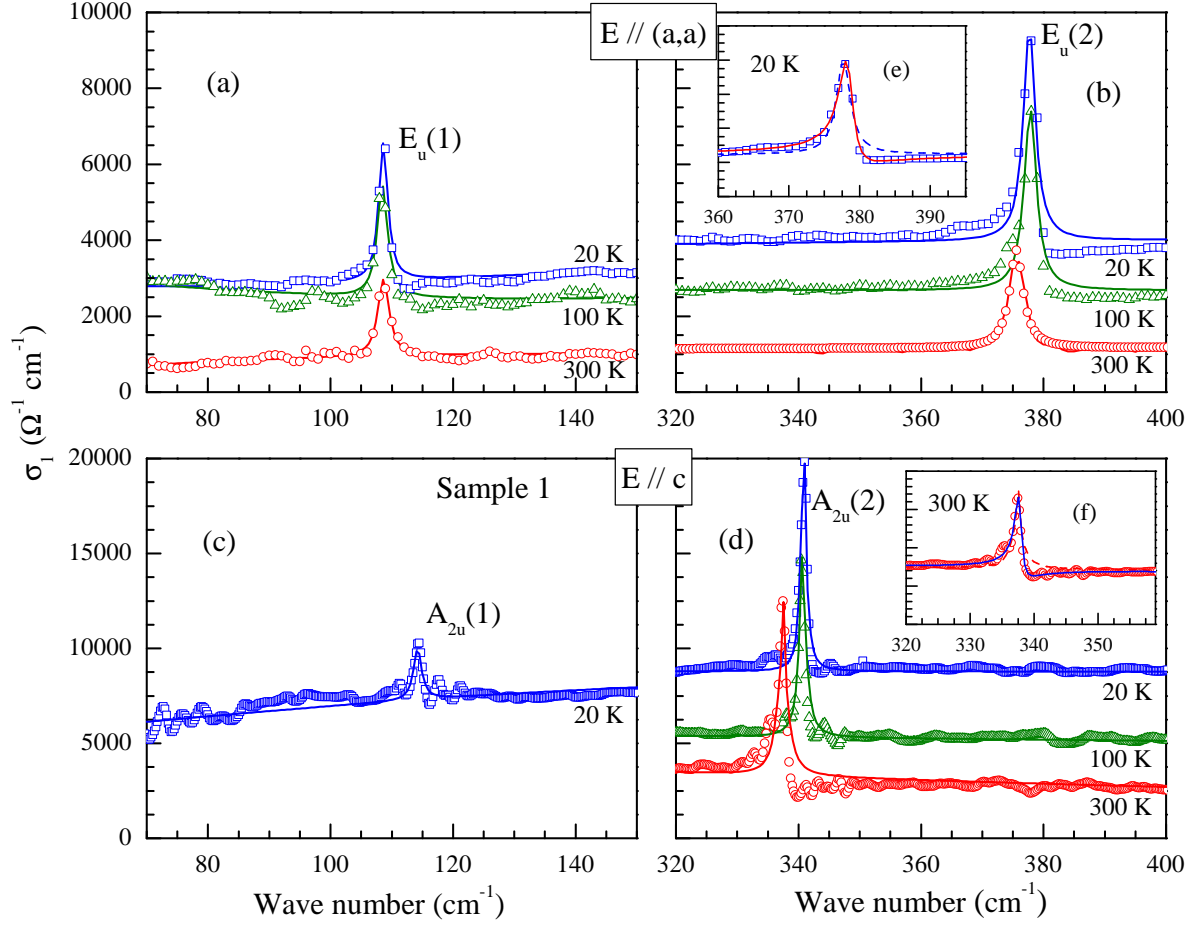


FIG. 7. (Color online) Optical conductivity centered around each phonon of  $\text{URu}_2\text{Si}_2$  at selected temperatures. Panels (a) and (b) are for light polarized on the  $(a,a)$  plane and panels (c) and (d) are for measurements along the  $c$ -direction. Symbols are the data and the lines are Drude-Lorentz fits as described in the text. Inset (e) shows the highest frequency  $E_u(2)$  mode at 20 K described by either a Lorentz oscillator (dashed line) or a Fano mode (solid line). Panel (f) is the equivalent to panel (e) for the highest frequency  $A_{2u}(2)$  mode at 300 K.

oscillators. This is a convenient way to parametrize the continuum but the values of the parameters do not carry a particular physical meaning and will not be discussed here. On top of this continuum we added a Lorentz oscillator for each phonon. One can see that the Lorentz oscillator describes reasonably well the phonon responses although the line shape is not perfect at a few temperatures, such as 20 K in panel (b) and 300 K in panel (d) (Fano line shape will be discussed later). Nevertheless, the Lorentz oscillator is very useful in analyzing the phonon spectral weight.

The spectral weight, characterizing the charge in a restricted spectral range, is defined as:

$$S_a^b = \int_{\omega_a}^{\omega_b} \sigma_1(\omega) d\omega. \quad (7)$$

When  $\omega_a \rightarrow 0$  and  $\omega_b \rightarrow \infty$ , one recovers the  $f$ -sum rule  $S = (\pi/2)(ne^2/m)$  ( $n$  is the total number of electrons,  $e$

is the electronic charge, and  $m$  the bare electronic mass). This rule states that the total integral under the real part of the optical conductivity is a constant independent of external parameters such as the temperature or pressure.

The spectral weight for a phonon within the Lorentz framework is:

$$S_p = \frac{\pi^2}{Z_0} \Delta\epsilon \Omega^2. \quad (8)$$

If phonons were decoupled from each other and from other excitations (*e.g.* electronic continuum), Eq. 8 should be temperature independent for each phonon.

Figure 8 shows the temperature dependence of the spectral weight of each phonon from Eq. 8, normalized by the total spectral weight for its respective polarization at room temperature, integrated up to  $2000 \text{ cm}^{-1}$ . Data for the lowest frequency  $A_{2u}$  is shown for completeness, but we do not have enough temperatures to draw any conclusion about this phonon.

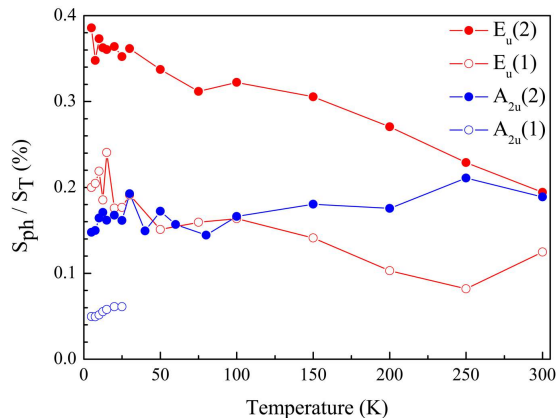


FIG. 8. (color online) Spectral weight of each phonon normalized by the spectral weight up to  $2000 \text{ cm}^{-1}$  calculated at room temperature.

The spectral weight of both  $E_u$  phonons almost doubles upon cooling the sample from room temperature to 5 K. The highest energy  $A_{2u}$  phonon also shows a temperature dependent spectral weight, albeit of smaller magnitude. Interestingly, for this phonon, the spectral weight decreases with decreasing temperature.

A temperature dependent spectral weight indicates that the effective charge of the phonons change with temperature. As the sum rule states that the total spectral weight must be conserved, this charge must be transferred from or to some other excitation. Because the spectral weight of the phonons correspond to less than 1% of the total spectral weight, we do not have enough resolution to pinpoint the energy (and hence the excitation) from which this charge is being transferred. However, the obvious candidate is the electronic continuum.

Indeed, let us go back to Fig. 7 and make a closer inspection on the phonon line shapes. In panel (e), we show the data for the highest  $E_{2u}$  phonon fitted by a Lorentz oscillator (dashed line) or a Fano mode (solid line) at 20 K. Only the latter properly describes the asymmetry observed in the measured data. This is the hallmark of an electron-phonon coupling and substantiates our claim that the phonon charge is changing due to a spectral weight transfer with the electronic continuum. Panel (f) shows that the same effect is present in the highest energy  $A_{2u}$  mode at 300 K.

Using the Fano mode fitting, we first extract the temperature dependence of the phonons energy normalized to their value at 300 K as presented Figure 9. At 300 K, the two  $E_u$  phonon modes are seen at  $108.7$  and  $375.6 \text{ cm}^{-1}$ , and the highest  $A_{2u}$  phonon mode at  $337.8 \text{ cm}^{-1}$ . Whereas the  $E_u(2)$  and  $A_{2u}(2)$  phonon modes exhibit the expected hardening when cooling down, the  $E_u(1)$  phonon mode shows constant energy down to  $\sim 20 \text{ K}$  and a small hardening of  $\sim 0.2 \%$  upon entering the HO phase. Even if only this low energy phonon  $E_u(1)$  has a singular temperature dependence, the  $E_u(2)$  and  $A_{2u}(2)$  phonon

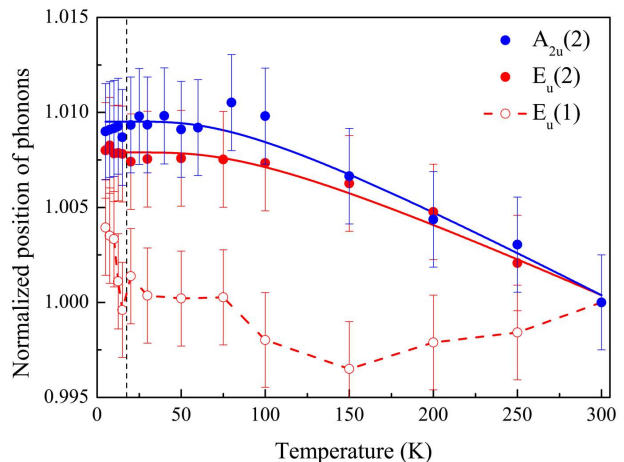


FIG. 9. (Color online) Temperature dependence of the frequency of  $A_{2u}(2)$ ,  $E_u(1)$  and  $E_u(2)$  phonon modes normalized to their value at 300 K. Lines are fits with a single anharmonic model (see Section III D). The vertical black dashed line marks the transition into the hidden order.

modes exhibit Fano line shape with peculiar temperature dependence, again evidencing that a complex electron-phonon coupling is in play in  $\text{URu}_2\text{Si}_2$ .

Fig. 10 shows the temperature behavior for the Fano-Wigner-Breit parameter for both  $E_u$  ((1) at  $108 \text{ cm}^{-1}$  and (2) at  $378 \text{ cm}^{-1}$ ) and the highest energy  $A_{2u}(2)$  (at  $340 \text{ cm}^{-1}$ ) phonons. The  $q^{-2}$  parameter for mode  $E_u(2)$  shows a behavior similar to its effective charge. Both quantities increase almost featurelessly with decreasing temperature. This joint behavior corroborates the electron-phonon coupling for this mode. Whereas we observe a clear drop in  $q^{-2}$  at the hidden order transition for the mode  $E_u$ , a drop which is directly related to the loss of carriers number at  $T_0$ , we cannot pinpoint a particular change of coupling in the paramagnetic state.

The phonons  $E_u(1)$  and  $A_{2u}(2)$ , on the other hand, show a striking change of regime close to the Kondo transition where coherent transport develops.  $E_u(1)$  has a very small, yet finite,  $q^{-2}$  at high temperatures. Close to the Kondo temperature it suddenly increases and the phonon develops an asymmetric shape. The opposite is observed for phonon  $A_{2u}(2)$ , which has an asymmetric shape and a large  $q^{-2}$  value above the Kondo temperature.

The temperature dependence of  $q^{-2}$  probes the variation of the continuum density of states close to the phonon energy. A decrease in  $q^{-2}$  indicates then that the density of states close to the phonon energy becomes smaller, *i.e.*, gapped. The optical conductivity results on the  $A_{2u}$  mode indicate that we would have a gapped system along  $k_z$  around  $40 \text{ meV}$  in the Kondo regime. Phonon  $E_u(1)$ , conversely, may indicate that the system is gapped or with strongly depleted density of states on the  $(k_x, k_y)$  plane at about  $12 \text{ meV}$  but this gap closes



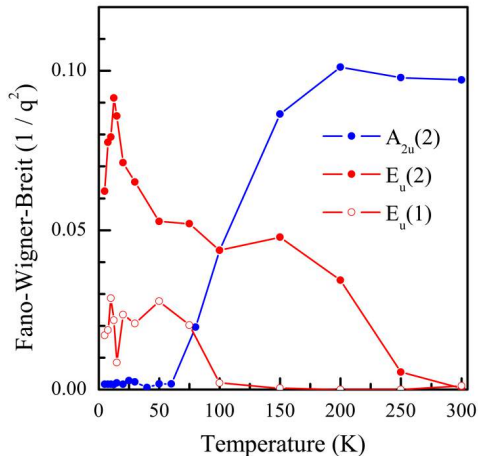


FIG. 10. (color online) Temperature dependence of Fano-Wigner-Breit  $q^{-2}$  parameter for both  $E_u$  and the highest frequency  $A_{2u}$  phonons. When an electron-phonon coupling occurs, the Fano-Wigner-Breit  $q^{-2}$  parameter becomes different from zero.

below the Kondo temperature or more generally the electronic density of state is enhanced when entering into the Kondo liquid regime.

Such observation of a temperature dependent Fano shape of a phonon mode in metallic Kondo systems has already been reported in  $\text{CeCoIn}_5$  by Raman scattering<sup>49</sup>. Indeed, according to their study of the lattice dynamics and electronic Raman response of  $\text{CeCoIn}_5$ , the entrance into the Kondo liquid regime below the crossover temperature  $T^* \sim 45$  K manifests by the divergence of the Fano coefficient of the  $A_{1g}$  phonon and by the significant drop of the scattering rate of the electronic scattering background. Both have been related to the enhancement of the electronic density of states due to the hybridization of 4f electrons with the conduction band. However the behavior as measured on the  $A_{2u}(2)$  mode in  $\text{URu}_2\text{Si}_2$  and even more the concomitant opposite behaviors of two phonons  $A_{2u}(2)$  and  $E_u(1)$  within the same compounds is striking and has never been reported to our knowledge. Most probably, this points to strongly momentum-dependent Kondo physics in  $\text{URu}_2\text{Si}_2$ , which affect distinctively both phonon modes with movements into different and perpendicular planes, namely the (x,y) and (z) planes.

## V. PHONONS AND MAGNETIC EXCITATIONS STUDIES BY INELASTIC NEUTRON SCATTERING

### A. Experimental Details

The phonon spectrum of  $\text{URu}_2\text{Si}_2$  was investigated by Inelastic Neutron Scattering (INS) at the Institute Laue-

Langevin. The first experiment was performed on the thermal neutron three axis spectrometer IN8. In the first configuration, the initial beam is provided by a double focusing Si monochromator ( $\text{Si}(1,1,1)$ ) and the scattered beam is analyzed by a double focusing Pyrolytic Graphite (PG) analyzer ( $\text{PG}(0,0,2)$ ) with fixed  $k_F = 2.662 \text{ \AA}^{-1}$ . In the second configuration, the initial beam is provided by a double focusing Cu monochromator ( $\text{Cu}(2,0,0)$ ) and the scattered beam is analyzed as previously but with fixed  $k_F = 4.1 \text{ \AA}^{-1}$ . This second configuration is used to investigate high energy modes. The second experiment was performed on the thermal neutron three axis spectrometer IN22 where the initial beam is provided by a double focusing PG monochromator ( $\text{PG}(0,0,2)$ ) and the scattered beam is analyzed by a double focusing PG analyzer ( $\text{PG}(0,0,2)$ ) with fixed  $k_F = 2.662 \text{ \AA}^{-1}$ . For these two experiments, the sample is a cylinder of diameter 4.5 mm and of length 8 mm along the  $a$ -axis; the scattering plane is defined by (1,0,0) and (0,0,1). The third experiment was performed on IN22 in polarized neutron setup with Heussler monochromator and analyzer with fixed  $k_F = 2.662 \text{ \AA}^{-1}$ . The neutron polarization is kept along the neutron path by guide fields and by an Helmholtz coil around the sample ; a Mezei flipper is placed before the analyzer. The experiment was performed with the neutron polarization parallel to the scattering vector ( $\mathbf{P} // \mathbf{Q}$ ). With this configuration, all the magnetic scattering appears in the Spin Flip (SF) channel while the phonon scattering appears in the Non Spin Flip (NSF) channel. For this experiment, the sample is a cylinder of diameter 4.5 mm and of length 12 mm along the  $c$ -axis and the scattering plane is defined by (1,0,0) and (0,1,0). In all measurements, the sample was inside an helium-4 flow cryostat covering the range 2-300 K. A PG filter was always placed in the scattered beam in order to remove higher order contamination. (Note for comparison between Raman, IR and neutron scattering that  $1 \text{ meV} = 8.06 \text{ cm}^{-1}$ ).

### B. RESULTS

In the present paper, the scattering vector  $\mathbf{Q}$  is decomposed into  $\mathbf{Q} = \mathbf{G} + \mathbf{q}$ , where  $\mathbf{G}$  is a reciprocal lattice wave vector and  $\mathbf{q}$  is the wave-vector of the excitation. The cartesian coordinates of  $\mathbf{q} = (h, k, l)$  are expressed in reciprocal lattice units (r.l.u.). Representative phonon spectra measured on IN8 are shown in Figure 11(a) for  $\mathbf{Q} = (0, 0, 5.25)$ . The two peaks at 11.8 and respectively 17.5 meV correspond to longitudinal acoustic (LA) and respectively longitudinal optic (LO) modes. Fits of the data are made at  $T = 300$  K using a flat background and a damped harmonic oscillator for the scattering function. The data at 2 K and 60 K are described by using the parameters obtained at 300 K except the intensity that is rescaled by the Bose factor. This procedure allows us to spot anomalous temperature behavior of the phonons.

The overall phonon modes measured along  $[0,0,1]$ ,

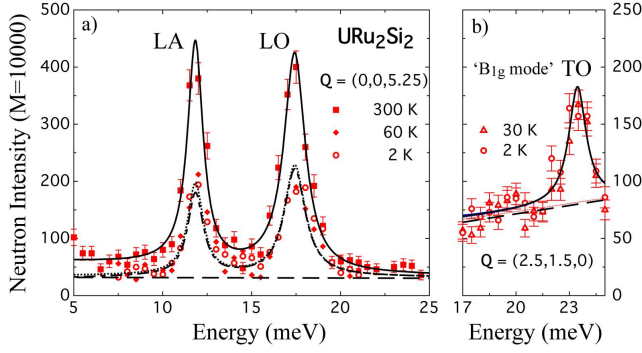


FIG. 11. (Color online) Inelastic Neutron Scattering phonon spectra measured for (a):  $\mathbf{Q}=(0, 0, 5.25)$  at  $T = 2, 60$  and  $300$  K performed on IN8 and (b):  $\mathbf{Q}=(2.5, 1.5, 0)$  at  $T = 2$  and  $30$  K performed on IN22. L and T, A and O stand for longitudinal and transverse, acoustic and optic, respectively. The TO mode belongs to the branch that corresponds to the  $B_{1g}$  mode at  $\mathbf{Q}=0$ . Lines are fits of the data with an harmonic oscillator lineshape and sloppy background. The neutron intensity is given for a normalized incident flux ( $M$ ) which corresponds to a counting time of approximately 80s.

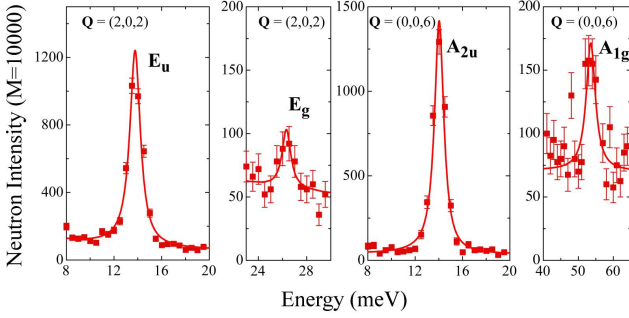


FIG. 12. (Color online) Inelastic Neutron Scattering phonon spectra at  $\Gamma$  point measured for  $\mathbf{Q}=(2, 0, 2)$  and  $\mathbf{Q}=(0, 0, 6)$  at  $T = 300$  K. The  $E_u$  and  $E_g$  phonon modes have been observed for  $\mathbf{Q}=(2, 0, 2)$  and  $A_{2u}$  and  $A_{1g}$  phonon modes for  $\mathbf{Q}=(0, 0, 6)$ . The neutron intensity is given for a normalized incident flux ( $M$ ) which corresponds to a counting time of approximately 80s for  $E_u$ ,  $E_g$ ,  $A_{2u}$  and 110s for  $A_{1g}$ . Lines are fits of the data with an harmonic oscillator lineshape.

$[1,0,0]$  and  $[1,1,0]$  directions do not show noticeable temperature dependence on cooling from  $300$  K to  $2$  K or on crossing  $T_0$ , except for a small expected hardening (See the LO branch in Figure 11 shifting a little to higher energy with decreasing temperature) which is a normal behavior of phonon on cooling. Although the softening of the  $B_{1g}$  mode seen by Raman scattering is too small ( $0.5\%$ ) to be detected by neutron measurement, a larger softening could occur at finite  $\mathbf{q}$ . Therefore a particular attention has been focused on the temperature dependence of the " $B_{1g}$ " branch for  $\mathbf{q} \neq 0$  in  $[0,0,1]$  and  $[1,1,0]$  directions. As presented for instance Figure 11(b) for  $\vec{Q}=(2.5,1.5,0)$ , no temperature difference has been observed between  $2$  K and  $30$  K.

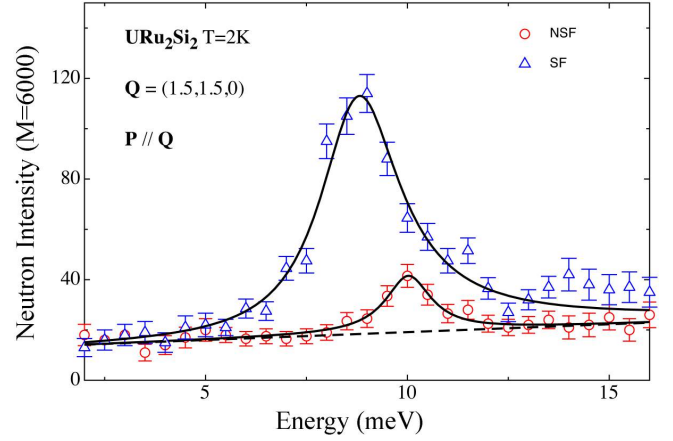


FIG. 13. (Color online) Polarized Inelastic Neutron Scattering spectra measured for  $\mathbf{Q}=(1.5, 1.5, 0)$  in the Non Spin Flip (NSF) and Spin Flip (SF) channels for  $T = 2$  K. Full lines are fits of the data with damped harmonic oscillator lineshape for the phonon and  $\omega$ -lorentzian lineshape for the magnetic excitation (For such a lineshape, see e.g.<sup>50</sup>). The dashed line indicates the background. The neutron intensity is given for a normalized incident flux which corresponds to a counting time ( $M$ ) of approximately 25min.

Figure 12 shows the four phonon modes  $E_u$ ,  $E_g$ ,  $A_{2u}$  and  $A_{1g}$  seen at  $\Gamma$  point by INS. A good agreement is found with the energy of these phonon modes measured by IR and Raman spectroscopy.

Further emphasis was given in the study of the phonons along the  $[1,1,0]$  direction by polarized neutron scattering following the report of anomalous phonon softening in this direction below  $T_0$ <sup>33</sup>.

Figure 13 shows a representative measurement performed on IN22, with the neutron polarization parallel to  $\mathbf{Q}$ , at X point in the Brillouin zone (See Figure 14) for  $\mathbf{Q}=(1.5, 1.5, 0)$  at  $T=2$  K for SF and NSF scattering. In the NSF scattering a phonon mode is observed at around  $10$  meV. In the SF channel, the large intensity peak centered at around  $8.7$  meV corresponds to the well-known magnetic excitation of  $\text{URu}_2\text{Si}_2$ . The peak position is in agreement with an early study performed along the  $[1,1,0]$  direction by Broholm et al.<sup>6</sup>. We therefore conclude the reported soft phonon mode<sup>33</sup> is in fact a magnetic excitation, an unambiguous result obtained by polarized INS.

Figure 14 summarize all the phonon and magnetic excitations dispersions we have measured along the main directions  $[1,0,0]$ ,  $[0,0,1]$  and  $[1,1,0]$ . As we have not observed any significant variation of the phonon energies as a function of temperature between  $300$  K and  $2$  K, we have reported the energy average of all measured temperature for each phonon mode. There is a fairly good agreement between the measurement and the calculation which includes the spin-orbit coupling (See section VI), except for few branches. The energy of the transverse (T) modes TA-z and TO-z (or " $A_{2u}(1)$ " branch) along  $[1,0,0]$  and TA-xy along  $[1,1,0]$  lines is  $\sim 20\%$  higher than what

is expected by the calculation.

We have not observed any magnetic excitations along  $[1,0,0]$  nearby  $\Gamma$  point. Then, most probably, the excitations reported by Broholm<sup>6</sup> in this  $\vec{k}$ -space zone are the optical phonon mode ('E<sub>u</sub>' or 'A<sub>2u</sub>' branches).

Furthermore, we report no particular anomaly of the phonon branches around  $Q_0$  and  $Q_1$  points where magnetic excitations are centered. No strong magneto-elastic coupling related to these magnetic modes is in play in URu<sub>2</sub>Si<sub>2</sub>.

## VI. THEORETICAL CALCULATIONS OF PHONON DISPERSION CURVES

The calculations have been performed using the density functional theory (DFT) implemented in the VASP software.<sup>51</sup> The electron potentials and wave-functions were obtained within the projector-augmented waves method<sup>52</sup> and the exchange and correlation energy was described by the generalized-gradient approximation.<sup>53</sup> The expansion of the single-particle plane waves has been restricted by the energy cutoff of 340 eV. The electronic and crystal structure have been optimized in the  $2 \times 2 \times 1$  supercell (40 atoms) with the periodic boundary conditions. We performed two types of calculations, with and without spin-orbit coupling (SOC), assuming in both cases the non-magnetic ground state. The optimization with the SOC gives slightly larger lattice constants than without SOC (see Table II). In both cases, the optimized lattice constants and the position of Si atoms ( $z$ ) show good agreement with the experimental values and the previous relativistic full-potential calculations<sup>54</sup>.

TABLE II. Lattice parameters obtained in calculations with and without SOC compared with the experimental values at  $T = 4.2$  K taken from Refs.<sup>1</sup> and<sup>55</sup>.

	$a$ (Å)	$c$ (Å)	$c/a$	$V$ (Å <sup>3</sup> )	$z$
SOC	4.143	9.589	2.31	164.59	0.374
no SOC	4.136	9.549	2.31	163.35	0.375
exp.	4.124	9.582	2.32	162.96	0.371

The phonon dispersion curves were obtained by using the direct method.<sup>56,57</sup> In this approach, the force constants are derived from the Hellmann-Feynman (HF) forces calculated *abinitio* by displacing atoms from equilibrium positions. Due to symmetry constraints, only three atoms (Si, Ru, and U) have to be displaced along two non-equivalent directions,  $x$  and  $z$ . In total, 12 independent calculations have been performed, including displacements in positive and negative directions. The phonon dispersions were calculated by the exact diagonalization of the dynamical matrix, obtained directly from the force constants.

The nature of the Raman and infrared-active vibrations are described in Fig. 1 and Table I. However, *abinitio* calculations of the phonon dispersion curves allow for a more detailed description of the actual atomic character of the vibrations. The atomic intensities for each phonon branch at the  $\Gamma$  point is shown in Table III. In this case, the intensity refers to the square of the vibrational amplitude of each atom for a given branch. This is particularly useful for the infrared-active A<sub>2u</sub> and E<sub>u</sub> modes, which in principle involve displacements of all of the atoms in the unit cell. The atomic intensity reveals that at the  $\Gamma$  point, the low-frequency A<sub>2u</sub> and E<sub>u</sub> modes involve mainly the U and Ru atoms, while the high-frequency A<sub>2u</sub> and E<sub>u</sub> modes are almost entirely Si in character with a slight involvement of the Ru atom.

In order to investigate possible anharmonic effects, two different sets of displacements, with  $u = 0.03$  Å and  $u = 0.06$  Å, were used to derive the HF forces. This approach would give us information about the possible deviation from the harmonic potential and it has been used previously to study the anharmonic behaviour in magnetite<sup>58</sup>. The results of both calculations are presented in Figure 15. Instead of phonon softening typical for an anharmonic potential, we observe the increase in energy at larger value of  $u$ . The effect is more apparent for the TA- $z$  and the lowest TO mode along the  $\Gamma X$  and  $\Gamma \Sigma Z$  directions and TA- $xy$  along the  $\Gamma Z$  direction. At the  $\Gamma$  point, two lowest infrared modes A<sub>2u</sub> and E<sub>u</sub> shift by +7% and +3%, respectively<sup>59</sup>. The energies of other modes depend on  $u$  very weakly.

To analyze the effect of the SOC, we have compared the results obtained with and without the SOC calculated for  $u = 0.06$  Å. As we see in Figure 15, the strongest effect is found for the lowest infrared A<sub>2u</sub> mode, which is shifted upward by 6.5% due to the SOC. The increase in energy in spite of larger lattice constants indicates a direct influence of the modified electronic structure on interatomic forces and phonon energies. Interestingly, the modes, which are strongly modified by the SOC, exhibit also the most pronounced dependence on  $u$ , and simultaneously they show the largest disagreement with the INS data (see Figure 14 and Table III). The results obtained with the SOC and  $u = 0.06$  Å, are slightly closer to the experimental points than the two other calculations.

## VII. GENERAL DISCUSSION AND CONCLUSION

Recently, orthorhombic distortion upon entering the HO has been measured by X-ray scattering by Tonegawa et al.<sup>29</sup> in disagreement with results by Amitsuka et al.<sup>60</sup>. Quantitative prediction of the effect of such distortion on the lattice dynamics would be of high interest as the phonon modes with displacements in the ( $a,a$ ) plane would be expected to broaden or split. We do not observe any splitting or broadening of the phonons measured by Raman scattering or by optical conductivity measure-

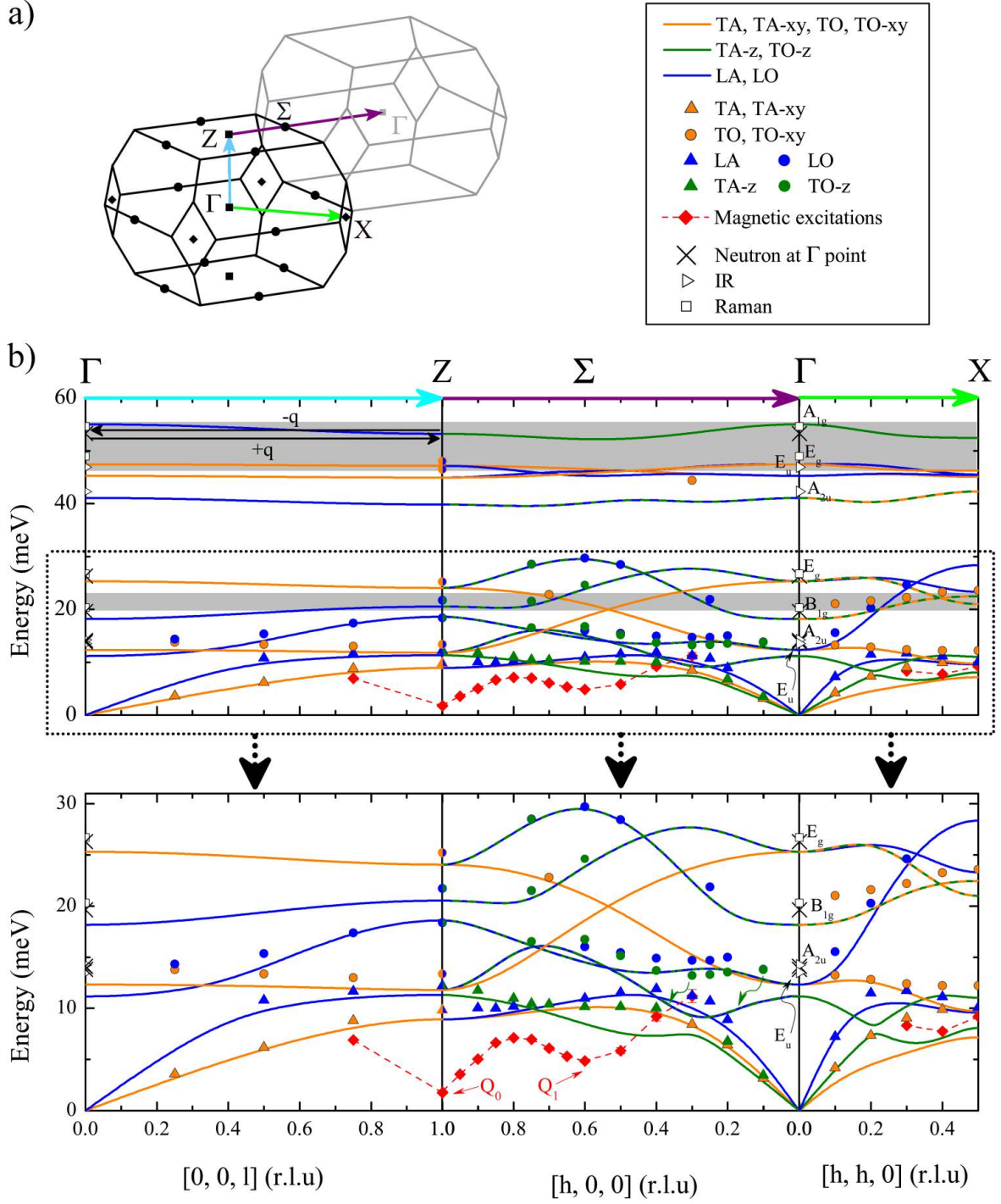


FIG. 14. (Color online) (a) Brillouin zone of the body centered tetragonal crystal structure of  $\text{URu}_2\text{Si}_2$  in the paramagnetic state. The arrows indicate the direction of the dispersion for the Inelastic Neutron Scattering (INS) measurements, as reported below. (b) Phonons and magnetic excitations (full red diamonds) dispersion along the  $\Gamma Z$  ( $[0,0,1]$ ),  $Z\Sigma$  ( $[1,0,0]$ ) and  $\Gamma X$  ( $[1,1,0]$ ) directions. Full circles and full upward triangles are INS data for the optical and acoustic branches, respectively. Empty symbols are data obtained in the zone center at  $\Gamma$ , with cross, open triangles and squares for INS, IR and Raman measurements, respectively. Dashed lines are guides to the eyes for the magnetic excitations dispersion. Solid lines corresponds to the *ab initio* GGA calculation with spin-orbit coupling and  $u=0.06 \text{ \AA}$  (See section VI). When the dispersion curve has a mixed character (for instance from LO (in  $\Gamma$ ) to TO-z (in  $Z$ ) along  $[1,0,0]$ ), the solid lines are bicolored. The black arrow points to the  $E_u(1)$  phonon mode measured by IR at  $\Gamma$  point. The green arrows indicate the calculated branch which corresponds to the measured points (green full circles). The grey areas indicate the energy range for all possible double phonon processes observed by Raman scattering (see Section III D). The two  $(\pm\vec{q})$  black arrows for the  $[0,0,1]$  direction show one possible double phonon process on the " $A_{1g}$ " branches.  $Q_0$  and  $Q_1$  correspond to the minima in magnetic excitation dispersion, known as commensurate and incommensurate excitations, respectively.



TABLE III. Phonon energies,  $E$ , for the phonon modes of URu<sub>2</sub>Si<sub>2</sub> in  $\text{cm}^{-1}$  at the  $\Gamma$  point obtained by Raman, infrared and inelastic neutron scattering measurements at the lowest temperature and, by *ab initio* studies at 0 K. We report the energies calculated with the spin-orbit coupling and  $u=0.06 \text{ \AA}$ . The ones calculated without the spin-orbit coupling and with  $u=0.06 \text{ \AA}$  are presented in parentheses. On the right: calculated atomic intensities of URu<sub>2</sub>Si<sub>2</sub> with spin-orbit coupling and displacements of  $u = 0.06 \text{ \AA}$  for the lattice modes at the  $\Gamma$  point. The  $\sum_{\mu,i} |\mathbf{e}_i(\mathbf{k}, j; \mu)|^2$  filter has been used to calculate how much the atom  $\mu$  is involved in the  $j$ th vibration.  $i = x, y, z$  and, here  $k=0$ .

Phonon modes at $\Gamma$ point	$E$ measured by			$E$ calculated	Atomic intensities		
	Raman spectroscopy	IR	neutron		U	Ru	Si
$A_{2u}$	/	114.8	111.2	90.1 (84.7)	0.52	0.42	0.06
$E_u$	/	109.1	113.6	99.5 (101.6)	0.52	0.42	0.06
$B_{1g}$	163.6	/	158.1 (leakage)	146.7 (144.2)	0	1.00	0.00
$E_g$	215.1	/	212.0	204.3 (206.6)	0	0.74	0.26
$A_{2u}$	/	340.8	/	331.5 (331.3)	0	0.17	0.83
$E_u$	/	378.6	/	365.3 (364.2)	0	0.17	0.83
$E_g$	394.1	/	/	382.9 (382.7)	0	0.26	0.74
$A_{1g}$	439.7	/	429.1	443.9 (459.7)	0	0.00	1.00

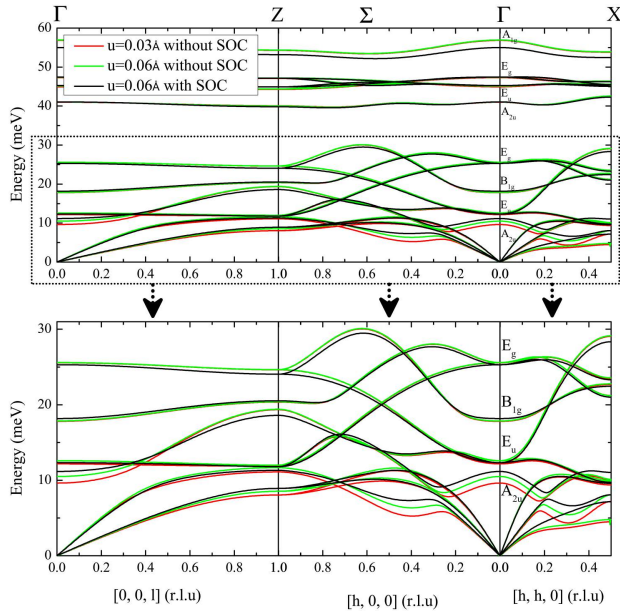


FIG. 15. (Color online) *Ab initio* calculation of the phonon dispersion curves along  $\Gamma Z$ ,  $\Gamma \Sigma Z$  and  $\Gamma X$  at 0 K. The parameter  $u$  sets for the displacements of the atoms. Increasing  $u$  from  $0.03 \text{ \AA}$  (red line) to  $0.06 \text{ \AA}$  (green line) is used to probe the effects of anharmonicity. Black line shows the calculation with spin-orbit coupling (SOC). The black line is the closest to the experimental results and is the one reported in Figure 14

ments, but a quantitative comparison with the predictions based on this recent measurement and the width across  $T_0$  as measured by optical spectroscopy would be necessary to definitively conclude.

Based on the observation of the same characteristic vector  $Q_0$  in the HO and AF phase<sup>25,26,61</sup> (Brillouin zone folding from a bct to st) and the absence of lattice distortions across  $T_0$ , Harima et al.<sup>62</sup> have selected 4 subgroups of the group 139 as candidates for the lower space group of the HO state ( $n^\circ 126, 128, 134$ , and  $136$ ); all have  $D_{4h}$  symmetry. Even without lattice distortion, across  $T_0$ , group theory predicts that new active phonon modes are allowed to emerge ( $B_{2g}$  phonon mode in the group  $n^\circ 126, 134$  and  $136$ ; only the group  $n^\circ 128$  doesn't have active  $B_{2g}$  phonon mode), some modes can be split ( $E_g$  or  $E_u$  modes) or new atoms are allowed to participate to the phonon movements (Uranium atoms in the  $E_g$  mode in group  $n^\circ 126$  and  $134$ ). None of these predictions have been observed here. Of course the effects of the electronic transition on the lattice dynamics might be very limited. Quantitative calculations on the lattice dynamics based on precise electronic ordering at  $T_0$  would be necessary to distinguish which effects would be sizable.

In conclusion, we have performed Raman scattering, optical conductivity, inelastic neutron scattering measurements and *ab initio* calculations focused on the lattice dynamic properties of URu<sub>2</sub>Si<sub>2</sub> in the 300 K - 2 K temperature range. We have measured all the optical phonon modes at the center of the Brillouin zone (BZ) and we have followed almost all phonon branches below 30 meV in the main symmetry directions of the BZ, together with their temperature dependencies. No particular effect of the entrance into the hidden order state has been detected except a change in the Fano shape of the  $E_u(2)$  phonon mode, a phonon which exhibits also a large increase of its spectral weight upon cooling from 300 K consistently with important electron-phonon coupling for this phonon. We attribute this behavior to the large loss of carriers upon entering the HO state. Other main effects have been obtained when entering into the Kondo regime. Indeed, we measure a small (0.5%) but sizable softening of the  $B_{1g}$  phonon mode below  $\sim 100 \text{ K}$ . Most probably a complex electron-phonon coupling is in play, related to the Kondo physics. This and the previously reported softening of the elastic constant of the same symmetry observed by ultrasound velocity measurements strongly suggest a  $B_{1g}$  symmetry-



breaking instability in the Kondo regime. The Kondo cross-over also impacts the infrared-active  $E_u(1)$  and  $A_{2u}(2)$  modes. Both of them present a Fano shape but whereas the  $A_{2u}(2)$  mode loses its Fano shape below 150 K, the  $E_u(1)$  mode acquires it below 100 K, in the Kondo cross-over regime. We attribute this behavior to strongly momentum-dependent Kondo physics. By drawing the full dispersion of the phonon modes and magnetic excitations, we conclude that there is no strong magneto-elastic coupling in  $\text{URu}_2\text{Si}_2$ . No remarkable temperature dependence has been obtained by INS including through the hidden order transition. Thanks to polarized inelastic neutron scattering, we were able to distinguish between phonon and magnon modes near the X and  $\Gamma$  points of the BZ, shedding light on previous reports<sup>33,63</sup>. The *ab initio* calculations of phonon energies and polarization vectors allowed us for the detailed analysis of phonon modes in the zone center and along the high-symmetry directions. A good agreement between the theory and experiment observed for most of dispersion curves indicates the itinerant character of  $5f$  electrons. The discrepancy found for the lowest TA and TO modes propagating in

the  $(a, b)$  plane may be caused by additional effects such as strong electron correlations, magnetic interactions or relativistic effects not fully included in the present calculations.

## ACKNOWLEDGMENTS

This work was supported by the Labex SEAM (Grant No. ANR-11-IDEX-0005-02) and by the french Agence Nationale de la Recherche (ANR PRINCESS). CCH is supported by the U.S. Department of Energy (DOE), Office of Basic Energy Sciences, Division of Materials Sciences and Engineering under Contract No. DE-AC02-98CH10886. The IT4Innovations National Supercomputing Center, VSB-Technical University, Ostrava, Czech Republic is acknowledged for providing the computer facilities under Grant Reg. No. CZ.1.05/1.1.00/02.0070. We thanks I. Paul, G. Knebel, C. Lacroix and P. Oppeneer for very fruitful discussions.

- 
- \* marie\_aude.measson[at]univ-paris-diderot.fr
- <sup>1</sup> T. T. M. Palstra, A. A. Menovsky, J. van den Berg, A. J. Dirkmaat, P. H. Kes, G. J. Nieuwenhuys, and J. A. Mydosh, *Physical Review Letters* **55**, 2727 (1985).
  - <sup>2</sup> J. A. Mydosh and P. M. Oppeneer, *Reviews of Modern Physics* **83**, 1301 (2011).
  - <sup>3</sup> J. Mydosh and P. Oppeneer, *Philosophical Magazine*, 1 (2014).
  - <sup>4</sup> W. Schlitz, J. Baumann, B. Pollit, U. Rauchschwalbe, H. M. Mayer, U. Ahlheim, and C. D. Bredl, *Zeitschrift für Physik B Condensed Matter* **62**, 171 (1986).
  - <sup>5</sup> A. de Visser, F. E. Kayzel, A. A. Menovsky, J. J. M. Franse, J. van den Berg, and G. J. Nieuwenhuys, *Physical Review B* **34**, 8168 (1986).
  - <sup>6</sup> C. Broholm, H. Lin, P. T. Matthews, T. E. Mason, W. J. L. Buyers, M. F. Collins, A. A. Menovsky, J. A. Mydosh, and J. K. Kjems, *Physical Review B* **43**, 12809 (1991).
  - <sup>7</sup> H. Kusunose and H. Harima, *Journal of the Physical Society of Japan* **80**, 084702 (2011).
  - <sup>8</sup> K. Haule and G. Kotliar, *Nature Physics* **5**, 796 (2009).
  - <sup>9</sup> H. Ikeda, M.-T. Suzuki, R. Arita, T. Takimoto, T. Shibauchi, and Y. Matsuda, *Nature Physics* **8**, 528 (2012).
  - <sup>10</sup> J. G. Rau and H.-Y. Kee, *Physical Review B* **85**, 245112 (2012).
  - <sup>11</sup> S. Fujimoto, *Physical Review Letters* **106**, 196407 (2011).
  - <sup>12</sup> P. S. Riseborough, B. Coqblin, and S. G. Magalhães, *Physical Review B* **85**, 165116 (2012).
  - <sup>13</sup> T. Das, *Physical Review B* **89**, 045135 (2014).
  - <sup>14</sup> C. Pépin, M. R. Norman, S. Burdin, and A. Ferraz, *Physical Review Letters* **106**, 106601 (2011).
  - <sup>15</sup> P. Chandra, P. Coleman, and R. Flint, *Nature* **493**, 621 (2013).
  - <sup>16</sup> S. Elgazzar, J. Ruzs, M. Amft, P. M. Oppeneer, and J. A. Mydosh, *Nature Materials* **8**, 337 (2009).
  - <sup>17</sup> F. Bourdarot, E. Hassinger, S. Raymond, D. Aoki, V. Taufour, L.-P. Regnault, and J. Flouquet, *Journal of the Physical Society of Japan* **79**, 064719 (2010).
  - <sup>18</sup> C. R. Wiebe, J. A. Janik, G. J. MacDougall, G. M. Luke, J. D. Garrett, H. D. Zhou, Y.-J. Jo, L. Balicas, Y. Qiu, J. R. D. Copley, Z. Yamani, and W. J. L. Buyers, *Nature Physics* **3**, 96 (2007).
  - <sup>19</sup> A. Villaume, F. Bourdarot, E. Hassinger, S. Raymond, V. Taufour, D. Aoki, and J. Flouquet, *Physical Review B* **78**, 012504 (2008).
  - <sup>20</sup> D. A. Bonn, J. D. Garrett, and T. Timusk, *Physical Review Letters* **61**, 1305 (1988).
  - <sup>21</sup> J. Schoenes, C. Schonenberger, J. J. M. Franse, and A. A. Menovsky, *Physical Review B* **35**, 5375 (1987).
  - <sup>22</sup> T. T. M. Palstra, A. A. Menovsky, G. J. Nieuwenhuys, and J. A. Mydosh, *Journal of Magnetism and Magnetic Materials* **54**, 435 (1986).
  - <sup>23</sup> P. Aynajian, E. H. da Silva Neto, C. V. Parker, Y. Huang, A. Pasupathy, J. Mydosh, and A. Yazdani, *Proceedings of the National Academy of Sciences* **107**, 10383 (2010).
  - <sup>24</sup> G. W. Scheerer, W. Knafo, D. Aoki, G. Ballon, A. Mari, D. Vignolles, and J. Flouquet, *Physical Review B* **85**, 094402 (2012).
  - <sup>25</sup> E. Hassinger, G. Knebel, T. D. Matsuda, D. Aoki, V. Taufour, and J. Flouquet, *Physical Review Letters* **105**, 216409 (2010).
  - <sup>26</sup> J. Buhot, M.-A. Méasson, Y. Gallais, M. Cazayous, G. Lapertot, D. Aoki, and A. Sacuto, *arXiv:1407.4651 [cond-mat]* (2014).
  - <sup>27</sup> R. Okazaki, T. Shibauchi, H. J. Shi, Y. Haga, T. D. Matsuda, E. Yamamoto, Y. Onuki, H. Ikeda, and Y. Matsuda, *Science* **331**, 439 (2011).
  - <sup>28</sup> S. Tonegawa, K. Hashimoto, K. Ikada, Y.-H. Lin, H. Shishido, Y. Haga, T. D. Matsuda, E. Yamamoto, Y. Onuki, H. Ikeda, Y. Matsuda, and T. Shibauchi, *Phys-*

- ical Review Letters **109**, 036401 (2012).
- <sup>29</sup> S. Tonegawa, S. Kasahara, T. Fukuda, K. Sugimoto, N. Yasuda, Y. Tsuruhara, D. Watanabe, Y. Mizukami, Y. Haga, T. D. Matsuda, E. Yamamoto, Y. Onuki, H. Ikeda, Y. Matsuda, and T. Shibauchi, *Nature Communications* **5**, 5188 (2014).
  - <sup>30</sup> S. L. Cooper, M. V. Klein, Z. Fisk, and J. L. Smith, *Physical Review B* **34**, 6235 (1986).
  - <sup>31</sup> T. Yanagisawa, S. Mombetsu, H. Hidaka, H. Amitsuka, M. Akatsu, S. Yasin, S. Zherlitsyn, J. Wosnitzer, K. Huang, and M. Brian Maple, *Journal of the Physical Society of Japan* **82**, 013601 (2013).
  - <sup>32</sup> K. Kuwahara, H. Amitsuka, T. Sakakibara, O. Suzuki, S. Nakamura, T. Goto, M. Mihalik, A. Menovsky, A. De Visser, and J. Franse, *Journal of the Physical Society of Japan* **66**, 3251 (1997).
  - <sup>33</sup> N. P. Butch, M. E. Manley, J. R. Jeffries, M. Janoschek, K. Huang, M. B. Maple, and J. W. Lynn, *arXiv preprint arXiv:1212.6238* (2012).
  - <sup>34</sup> W. Hayes and R. Loudon, *Scattering of Light by Crystals*, Dover Books on Physics (Dover Publications, 2004).
  - <sup>35</sup> D. Aoki, F. Bourdarot, E. Hassinger, G. Knebel, A. Miyake, S. Raymond, V. Taufour, and J. Flouquet, *Journal of Physics: Condensed Matter* **22**, 164205 (2010).
  - <sup>36</sup> J. Buhot, M.-A. Méasson, Y. Gallais, M. Cazayous, A. Sacuto, G. Lapertot, and D. Aoki, *Journal of the Korean Physical Society* **62**, 1427 (2013).
  - <sup>37</sup> P. G. Klemens, *Physical Review* **148**, 845 (1966).
  - <sup>38</sup> J. Menéndez and M. Cardona, *Physical Review B* **29**, 2051 (1984).
  - <sup>39</sup> U. Fano, *Physical Review* **124**, 1866 (1961).
  - <sup>40</sup> M. Cardona, *Light Scattering in Solids I: Introductory Concepts* (Springer Berlin Heidelberg, 1982).
  - <sup>41</sup> S. L. Cooper, M. V. Klein, M. B. Maple, and M. S. Torikachvili, *Physical Review B* **36**, 5743 (1987).
  - <sup>42</sup> D. Lampakis, D. Palles, E. Liarokapis, and J. Mydosh, *Physica B: Condensed Matter* **378-380**, 578 (2006).
  - <sup>43</sup> U. Nagel, T. Uleksin, T. Room, R. P. S. M. Lobo, P. Lejay, C. C. Homes, J. S. Hall, A. W. Kinross, S. K. Purdy, T. Munsie, T. J. Williams, G. M. Luke, and T. Timusk, *Proceedings of the National Academy of Sciences* **109**, 19161 (2012).
  - <sup>44</sup> W. T. Guo, Z. G. Chen, T. J. Williams, J. D. Garrett, G. M. Luke, and N. L. Wang, *Physical Review B* **85**, 195105 (2012).
  - <sup>45</sup> J. Levallois, F. Lévy-Bertrand, M. K. Tran, D. Stricker, J. A. Mydosh, Y.-K. Huang, and D. van der Marel, *Physical Review B* **84**, 184420 (2011).
  - <sup>46</sup> C. C. Homes, M. Reedyk, D. A. Cradles, and T. Timusk, *Applied Optics* **32**, 2976 (1993).
  - <sup>47</sup> L. Degiorgi, S. Thieme, H. R. Ott, M. Dressel, G. Grüner, Y. Dalichaouch, M. B. Maple, Z. Fisk, C. Geibel, and F. Steglich, *Zeitschrift für Physik B Condensed Matter* **102**, 367 (1997).
  - <sup>48</sup> L. C. Davis and L. A. Feldkamp, *Physical Review B* **15**, 2961 (1977).
  - <sup>49</sup> H. Martinho, P. G. Pagliuso, V. Fritsch, N. O. Moreno, J. L. Sarrao, and C. Rettori, *Physical Review B* **75**, 045108 (2007).
  - <sup>50</sup> J. Panarin, S. Raymond, G. Lapertot, J. Flouquet, and J.-M. Mignot, *Physical Review B* **84**, 052505 (2011).
  - <sup>51</sup> G. Kresse and J. Furthmüller, *Physical Review B* **54**, 11169 (1996).
  - <sup>52</sup> P. E. Blochl, *Physical Review B* **50**, 17953 (1994).
  - <sup>53</sup> J. P. Perdew, K. Burke, and M. Ernzerhof, *Physical Review Letters* **77**, 3865 (1996).
  - <sup>54</sup> P. M. Oppeneer, J. Ruzs, S. Elgazzar, M.-T. Suzuki, T. Durakiewicz, and J. A. Mydosh, *Physical Review B* **82**, 205103 (2010).
  - <sup>55</sup> G. Cordier, E. Czech, H. Schäfer, and P. Woll, *Journal of the Less Common Metals* **110**, 327 (1985).
  - <sup>56</sup> K. Parlinski, Z. Q. Li, and Y. Kawazoe, *Physical Review Letters* **78**, 4063 (1997).
  - <sup>57</sup> K. Parlinski, *Collection SFN* **12**, 161 (2011).
  - <sup>58</sup> M. Hoesch, P. Piekarczyk, A. Bosak, M. Le Tacon, M. Krisch, A. Kozłowski, A. M. Oleś, and K. Parlinski, *Physical Review Letters* **110**, 207204 (2013).
  - <sup>59</sup> In the case of smaller displacements  $u = 0.03 \text{ \AA}$  numerical values of forces are too small, which may be the origin of some numerical error, therefore, we present phonon energies  $c$  and dispersions obtained for  $u = 0.06 \text{ \AA}$ .
  - <sup>60</sup> H. Amitsuka, *Workshop on hidden order, superconductivity and magnetism in URu<sub>2</sub>Si<sub>2</sub>*, Leiden (2013).
  - <sup>61</sup> R. Yoshida, K. Tsubota, T. Ishiga, M. Sunagawa, J. Sonoyama, D. Aoki, J. Flouquet, T. Wakita, Y. Muraoka, and T. Yokoya, *Scientific Reports* **3**, 02750 (2013).
  - <sup>62</sup> H. Harima, K. Miyake, and J. Flouquet, *Journal of the Physical Society of Japan* **79**, 033705 (2010).
  - <sup>63</sup> C. Broholm, J. K. Kjems, W. J. L. Buyers, P. Matthews, T. T. M. Palstra, A. A. Menovsky, and J. A. Mydosh, *Physical Review Letters* **58**, 1467 (1987).